Communication

Mn Pulse ENDOR at 34 GHz of the S and S States of the Oxygen-Evolving Complex in Photosystem II

Leonid V. Kulik, Boris Epel, Wolfgang Lubitz, and Johannes Messinger

J. Am. Chem. Soc., **2005**, 127 (8), 2392-2393• DOI: 10.1021/ja043012j • Publication Date (Web): 05 February 2005

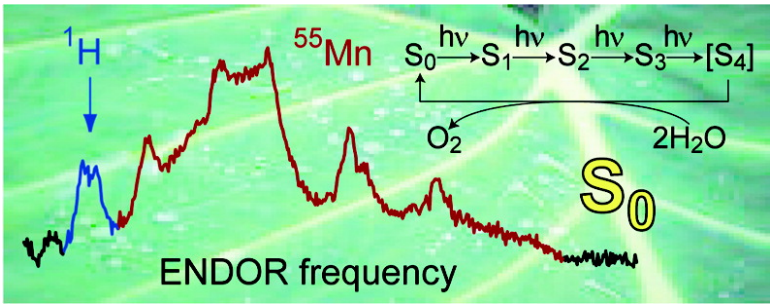

More About This Article

Additional resources and features associated with this article are available within the HTML version:

- Supporting Information
- Links to the 15 articles that cite this article, as of the time of this article download
- Access to high resolution figures
- Links to articles and content related to this article
- Copyright permission to reproduce figures and/or text from this article

View the Full Text HTML

J|A|C|S
COMMUNICATIONS

Published on Web 02/05/2005

^{55}Mn Pulse ENDOR at 34 GHz of the S_0 and S_2 States of the Oxygen-Evolving Complex in Photosystem II

Leonid V. Kulik,[§] Boris Epel, Wolfgang Lubitz,* and Johannes Messinger*

Max-Planck-Institut für Bioanorganische Chemie, Stiftstrasse 34-36, D-45470 Mülheim/Ruhr, Germany

Received November 19, 2004; E-mail: lubitz@mpi-muelheim.mpg.de; messinger@mpi-muelheim.mpg.de

Powered by light-induced charge separations that generate oxidizing equivalents of about +1.3 V, photosystem II (PSII) has the unique capability to oxidize water to molecular oxygen. Water splitting is catalyzed by a Mn_4O_xCa complex housed in a special protein environment that also controls proton movements and the access of water. This functional unit of PSII is referred to as the oxygen−evolving complex (OEC). PSII created the aerobic atmosphere on earth and may serve as a model for technical approaches to split water by sunlight, which is a prerequisite for a sustainable hydrogen economy. Despite the availability of crystal structures of PSII with 3.5 and 3.2 Å resolutions and of extensive EPR and EXAFS studies, the precise geometric and electronic structures of the various functional states of the Mn_4O_xCa complex are still unknown.[1−5] During the reaction sequence (Kok cycle) the OEC passes through five oxidation states (S states, S_0−S_4),[6] of which the S_0 and S_2 states have $S = {}^1/_2$ ground states. Continuous wave (CW) EPR has been used to study the electronic structures of these states,[7−10] but despite the rich hyperfine structures of the S_2 and S_0 EPR multiline signals, it has not been possible to uniquely determine the hyperfine interaction (HFI) tensors of the individual Mn ions in this way. For such complex spin systems, it is required to directly probe the Mn HFI parameters by ^{55}Mn pulse ENDOR spectroscopy. For technical reasons and due to the complex preparation procedure for concentrated S_0 state samples, such experiments were done so far only at X-band for the S_2 state; they gave the first reliable HFI parameters.[11] In this study we report ^{55}Mn pulse ENDOR spectra for the S_0 and S_2 states at Q-band frequency (34 GHz). Numerical analysis of our spectra (i) shows that all four Mn ions are magnetically coupled, (ii) allows a refinement of the HFI parameters for the S_2 state, (iii) provides the first reliable HFI tensors for the S_0 state, and (iv) leads to a suggestion for the Mn oxidation states in S_0 and S_2.

PSII membranes were prepared according to standard procedures[8] and washed several times after the Triton treatment to completely remove starch. S_2 state samples were obtained by concentrating dark-adapted PSII membranes containing 250 μM PPBQ (phenyl-*p*-benzoquinone) and 1 mM EDTA in 3 mm quartz tubes by centrifugation (~25 mg of chlorophyll/mL final) and subsequent 200 K illumination. S_0 state samples were prepared using the three-flash/FCCP approach described previously.[8,12] The samples were finally concentrated by centrifugation in the Q-band EPR tubes. After completion of the ^{55}Mn ENDOR experiments, the S_0 state population was determined to be 65 ± 5% (the rest being S_1) on the basis of the amplitude of the S_2 EPR multiline signal generated by 200 K illumination compared to that of S_2 control samples. All samples contained 3% (v/v) methanol.

The experiments were performed on a Bruker ESP-580 Q-band pulse EPR spectrometer equipped with a home-built ENDOR cavity. The pulse ENDOR experiments were performed using SpecMan control software that varies the radio frequency (rf) randomly in the desired range. This leads to a decrease of the rf-induced heat accumulation in the resonator and in turn to a reduction of heating artifacts.

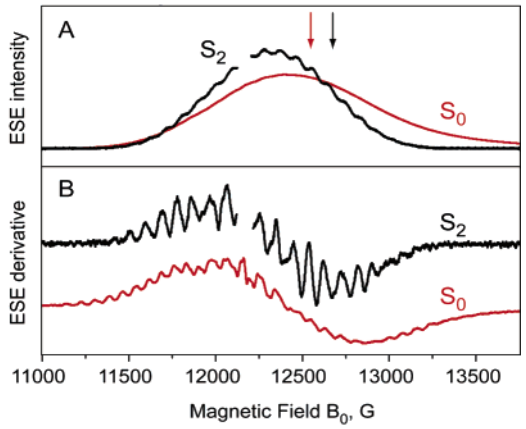

Figure 1. Q-band echo-detected EPR spectra (light minus dark) of the S_2 and S_0 states (A) and their numerical pseudomodulation with 20 G amplitude, which gives CW EPR-like derivative spectra (B). T = 4.5 K, mw π/2-pulse 32 ns, τ = 260 ns, ν_{mw} = 33.850 GHz (S_2 state), 34.123 GHz (S_0 state). The spectra of the S_2 state are shifted by 100 G to higher magnetic field to compensate for the mw frequency difference. The pulse repetition time was 1 ms (S_2 state) and 12 μs (S_0 state). The arrows indicate the magnetic field positions where ^{55}Mn ENDOR spectra were taken (see Figure 2). In the S_2 state spectra, the sharp signal of the tyrosine D radical of PSII at $g \approx 2$ is removed for clarity. This signal is practically absent for the S_0 state sample due to chemical reduction by FCCP.

Figure 1A shows the two-pulse echo-detected EPR spectra of the S_2 and S_0 states (light minus dark difference). A comparison reveals that the S_0 signal is ~500 G broader and that the extra width mainly stems from the high-field wing. This indicates substantial g-anisotropy in the S_0 state and shows that g_{iso} of the S_0 state is smaller than g_{iso} of the S_2 state. The CW EPR-like derivative spectra of Figure 1B are produced by numerical pseudomodulation of the field sweeps (Figure 1A) using a 20 G amplitude. This procedure allows a closer inspection of the hyperfine structure. For the S_0 state, this is the first report of a CW-like Q-band EPR spectrum. The total width is about 2500 G, and at least 26 lines are resolved. At the low-field side the average splitting is about 78 G, and at the high-field side it is 84 G. The overall similarity to the well-known S_0 state CW EPR X-band spectrum confirms that the Q-band two-pulse echo originates from the S_0 state. An inversion−recovery measurement of the spin lattice relaxation time T_1 for the S_0 state (data not shown) gives $T_1 \approx 9$ μs at 4.5 K, which is about 100 times faster than the T_1 of the S_2 state.[13] This is in line with previous reports that the S_0 state has a higher half-saturation power than the S_2 state.[9,14]

The black lines in Figure 2 show the ^{55}Mn ENDOR spectra of the S_2 and S_0 states that were recorded at the magnetic field

[§] Permanent address: Institute of Chemical Kinetics and Combustion, Institutskaya 3, 630090 Novosibirsk, Russia.

10.1021/ja043012j CCC: $30.25

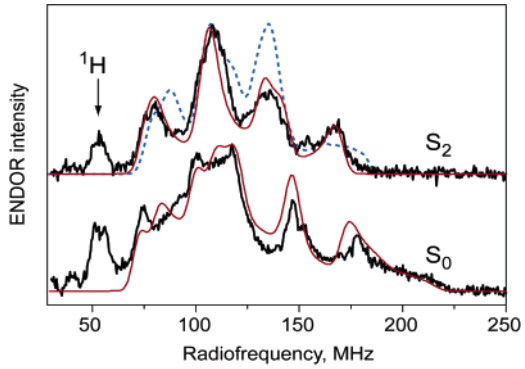

Figure 2. ^{55}Mn pulse ENDOR spectra at Q-band of the S_2 and S_0 states (black) and simulations using either the parameters of Table 1 (red) or those determined previously by Peloquin et al.[11] on the basis of X-band ^{55}Mn ENDOR (broken blue line). The Davies ENDOR sequence was used with a radio frequency (rf) π-pulse duration of 5 μs (S_2 state) and 4 μs (S_0 state). Temperature and other conditions are the same as in Figure 1. B_0 = 12600 G (S_2 state) and 12550 G (S_0 state).

Table 1. Principal Values of HFI Tensors (Absolute Values) of Individual ^{55}Mn Ions Used for Simulation of the ^{55}Mn ENDOR Spectra of the OEC

	S_2 state		S_0 state	
	$A_\perp$, MHz	$A_\parallel$, MHz	$A_\perp$, MHz	$A_\parallel$, MHz
Mn_A	235	265	270	200
Mn_B	185	245	190	280
Mn_C	310	265	320	400
Mn_D	175	230	170	240

positions indicated by the arrows in Figure 1A. Similar results were obtained at other field positions, which indicates a negligible orientation selection (data not shown). The S_2 state spectrum spans from 70 to 180 MHz, which is 20 MHz wider than at X-band. This difference is readily explained by the increased Zeeman frequency of the Mn nuclei (13 MHz at Q-band vs 3 MHz at X-band). The spectrum of the S_0 state is broader than that of the S_2 state; a weak shoulder extends to 220 MHz. Its low-frequency edge is probably at 70 MHz, but there is the possibility that a weak wing spans below the proton peak down to ~50 MHz. Scans up to 400 MHz do not reveal any additional signals.

Because of the small orientation selection, the mean ^{55}Mn ENDOR frequency (the "center of gravity" of the spectrum) equals approximately half of the absolute value of the isotropic Mn HFI constants averaged over the four Mn nuclei, $\langle|A_{iso}|\rangle/2$. For theoretical spectra, this procedure has shown a precision of better than 1%. Analysis of the experimental ^{55}Mn ENDOR spectrum of the S_0 state gives $\langle|A_{iso}|\rangle$ = 250 MHz. In the case of isotropic Mn HFI tensors, their contribution to the width of the EPR spectrum is $W'_{HFI} = 5N\langle|A_{iso}|\rangle$, where N is the number of Mn nuclei. Any anisotropy in the HFI increases this value. The simulation shows that this increase is about 12% for the S_0 state (Table 1). The total width of the X-band S_0 state EPR spectrum is W_T = 6160−6700 MHz (g = 2).[8] With N = 4, we obtain W_{HFI} = 5600 MHz. The difference between W_{HFI} and W_T can be explained by a g-tensor anisotropy of $\Delta g \approx 0.1-0.2$, which is in the expected range. A trinuclear or binuclear origin for the S_0 multiline requires a much larger g-tensor anisotropy of $\Delta g \approx 0.4-0.5$ or 0.65−0.75, respectively. This strongly disfavors such proposals. For the S_2 state, the comparison of W_T = 5400 MHz and W_{HFI} = 4700 MHz (Q-band) gives an upper limit of $\Delta g \approx 0.04$ for N = 4, which agrees with the previously reported values of $\Delta g \approx 0.02-0.04$[2,11,15] and further supports the idea that all four Mn nuclei are magnetically coupled in both states.

The red lines in Figure 2 show numerical simulations of the ^{55}Mn ENDOR spectra, performed using second-order perturbation theory.[16] Only the allowed transitions were taken into account. For simplicity, axial g-tensors and Mn HFI tensors with coinciding directions for the symmetry axes were assumed, and Mn nuclear quadrupole interaction (NQI) was excluded (Table 1). Within this simple model, the precision of the simulation is ±10 MHz. Since the signs of HFI constants cannot be determined by ENDOR simulations, only their absolute values are presented. We used $g_\perp$ = 1.97, $g_\parallel$ = 1.99 for the S_2 state and $g_\perp$ = 1.99, $g_\parallel$ = 1.89 for the S_0 state (see above). However, the simulated ^{55}Mn ENDOR spectrum is essentially insensitive to the variation of the principal values of the g-tensor. The HFI parameters for the S_2 state are close to those derived previously on the basis of X-band ^{55}Mn ENDOR; a simulation using these previously reported parameters is shown for visual comparison as the broken blue line in Figure 2.[11]

Overall, surprisingly similar ^{55}Mn ENDOR spectra (Figure 2) and HFI parameters (Table 1) are found in this study for the S_0 and S_2 states. This appears to favor Mn_4(III, III, III, IV) and Mn_4(III, IV, IV, IV) as oxidation states for the S_0 and S_2 states, respectively, over alternative assignments that contain one Mn(II) in the S_0 state. This idea and possible structural models for the Mn_4O_xCa complex will be tested in a forthcoming publication, where the obtained HFI parameters will be used together with various spin-coupling schemes for the simulation of the hyperfine structures of the S_2 and S_0 EPR signals.

Acknowledgment. Leonid Kulik is grateful to the Alexander von Humboldt Foundation for financial support. This work was supported by the Max Planck Society and by the DFG (Me 1629/2-3).

References

(1) Messinger, J. *Phys. Chem. Chem. Phys.* **2004**, *6*, 4764−4771.
(2) Carell, T. G.; Tyryshkin, A. M.; Dismukes, G. C. *J. Biol. Inorg. Chem.* **2002**, *7*, 2−22.
(3) McEvoy, J. P.; Brudvig, G. W. *Phys. Chem. Chem. Phys.* **2004**, *6*, 4754−4763.
(4) Ferreira, K. N.; Iverson, T. M.; Maghlaoui, K.; Barber, J.; Iwata, S. *Science* **2004**, *303*, 1831−1838.
(5) Biesiadka, J.; Loll, B.; Kern, J.; Irrgang, K.-D.; Zouni, A. *Phys. Chem. Chem. Phys.* **2004**, *6*, 4733−4736.
(6) Kok, B.; Forbush, B.; McGloin, M. *Photochem. Photobiol.* **1970**, *11*, 457−476.
(7) Dismukes, G. C.; Siderer, Y. *Proc. Natl. Acad. Sci. U.S.A.* **1981**, *78*, 274−278.
(8) Messinger, J.; Robblee, J. H.; Yu, W. O.; Sauer, K.; Yachandra, V. K.; Klein, M. P. *J. Am. Chem. Soc.* **1997**, *119*, 11349−11350.
(9) Messinger, J.; Nugent, J. H. A.; Evans, M. C. W. *Biochemistry* **1997**, *36*, 11055−11060.
(10) Åhrling, K. A.; Peterson, S.; Styring, S. *Biochemistry* **1997**, *36*, 13148−13152.
(11) Peloquin, J. M.; Campbell, K. A.; Randall, D. W.; Evanchik, M. A.; Pecoraro, V. L.; Armstrong, W. H.; Britt, R. D. *J. Am. Chem. Soc.* **2000**, *122*, 10926−10942.
(12) Robblee, J. H.; Messinger, J.; Cinco, R. M.; McFarlane, K. L.; Fernandez, C.; Pizarro, S. A.; Sauer, K.; Yachandra, V. K. *J. Am. Chem. Soc.* **2002**, *124*, 7459−7471.
(13) Lorigan, G. A.; Britt, R. D. *Biochemistry* **1994**, *33*, 12072−12076.
(14) Peterson, S.; Åhrling, K. A.; Styring, S. *Biochemistry* **1999**, *38*, 15223−15230.
(15) Zheng, M.; Dismukes, G. C. *Inorg. Chem.* **1996**, *35*, 3307−3319.
(16) Sturgeon, B. E.; Ball, J. A.; Randall, D. W.; Britt, R. D. *J. Phys. Chem.* **1994**, *98*, 12871−12883.

JA043012J